Electrochimica Acta 56 (2011) 10253–10258

Contents lists available at SciVerse ScienceDirect

Electrochimica Acta

journal homepage: www.elsevier.com/locate/electacta

Electro-oxidation of ethylene glycol on nanoporous Ti–Cu amorphous alloy

Cuijie Chen[a], Shengli Zhu[a,b,*], Xianjin Yang[a,b], Lele Pi[a], Zhenduo Cui[a]

[a] School of Materials Science and Engineering, Tianjin University, Tianjin 300072, China
[b] Tianjin Key Laboratory of Composite and Functional Materials, Tianjin 300072, China

ARTICLE INFO

Article history:
Received 10 May 2011
Received in revised form 3 September 2011
Accepted 7 September 2011
Available online 16 September 2011

Keywords:
Ti–Cu amorphous alloy
Nanoporous structure
Electrocatalysis
Ethylene glycol
Heat treatment

ABSTRACT

This work describes ethylene glycol (EG) electro-oxidation over nanoporous structure catalyst prepared by dealloying Ti–Cu amorphous alloy. Scanning electron microscopy (SEM) was used to characterize nanoporous catalysts. Electrocatalytic performances in acid and alkaline mediums were measured by cyclic voltammetry (CV), chronoamperometry (CA) and electrochemical impedance spectroscopy (EIS). The results showed that nanoporous Ti–Cu amorphous alloy exhibited apparent electrocatalytic ability in terms of higher oxidation current in CV and CA curves comparing to raw Ti–Cu amorphous alloy. Electro-oxidation of EG took place more easily in alkaline medium than that in acid medium. In acid medium, heat treatment improved the electrocatalytic activity of nanoporous catalyst. In alkaline medium, heat treatment played an enhancing role below 0.1 V and a depressing role above 0.1 V. Possible electro-oxidation mechanism of EG was also discussed.

1. Introduction

Electrocatalytic oxidation of small organic molecules gains much attention all over the world, owning to the development of direct fuel cells which are new promising power sources in the future [1,2]. Ethylene glycol (EG) is hopeful to substitute methanol as direct alcohols fuel cell, due to its higher energy density, higher reaction activity, lower toxicity, and lower membrane permeation comparing to methanol [3,4].

Recently, carbon-supported noble electrodes were generally used as electrocatalysts [5–8]. Meanwhile, carbon nanotubes, carbon nanofibers and TiO_2 nanotubes were utilized as attractive supports for metal catalysts, due to their large surface areas, high electrical conductivities, and high thermal, mechanical, chemical, and electrochemical stabilities [9–16]. The above materials enable high dispersion of catalyst nanoparticles, facilitate electrons transfer, and allow fast mass transport of reactants and products at the fuel cell electrodes, resulting in better device performance [17].

Additionally, noble metal (Pt, Pd and Au) and its alloy nanostructures were extensively investigated in electrocatalytic oxidation of small organic molecules [1,2,18–27]. Particularly, much attention was paid to nanoporous metallic materials, especially nanoporous Au, Pt, and Ni, in view of their potential applications in catalysis [28–30].

Nanoporous metals were obtained from selective dissolution of the relatively active phase out of Ag–Au [31–33], Pt–Cu [34,35], Al–Ag [36,37], and Mg–Cu [38] alloys. This process is called dealloying. In addition, amorphous alloys, such as Pt–Si, Pd–Ni–P, were chosen as starting alloys due to their monolithic phase with homogeneous composition [39–42]. Nanoporous metallic catalysts with large specific surface areas can greatly improve the utilization of surface active sites and promote chemical reactions [28].

A facile method was developed to synthesize nanoporous metals through dealloying Ti–Cu amorphous alloy in HNO_3 aqueous solution [43]. This work aims to systematically investigate the electrocatalytic activities of nanoporous Ti–Cu amorphous alloy towards EG electro-oxidation in acid and alkaline mediums. Possible electro-oxidation mechanism of EG is discussed.

2. Experiments

Original nanoporous Ti–Cu amorphous alloy was prepared as described in reference [43]. Briefly, the raw $Ti_{30}Cu_{70}$ (nominal atomic ratio) amorphous ribbon was prepared using a melt-spinning method. And the dealloying process took place in a conventional three-electrode cell in 5.36 M HNO_3 electrolyte solution at 343 K. Raw $Ti_{30}Cu_{70}$amorphous ribbon was utilized as working electrode. Platinum net and a saturated calomel electrode (SCE) were served as counter and reference electrodes, respectively. Applied potential was 1.0 V vs. SCE and reaction time was 10,800 s [43]. Heat treated sample was prepared by annealing the original sample at 573 K for 30 min, and then being ultrasonic cleaned with distilled water and dried at room temperature. Raw Ti–Cu amorphous alloy, as-prepared original and heat treated nanoporous

* Corresponding author at: School of Materials Science and Engineering, Tianjin University, Tianjin 300072, China. Tel.: +86 22 27402494.
E-mail address: slzhu@tju.edu.cn (S. L. Zhu).

0013-4686/$ – see front matter © 2011 Elsevier Ltd. All rights reserved.
doi:10.1016/j.electacta.2011.09.018

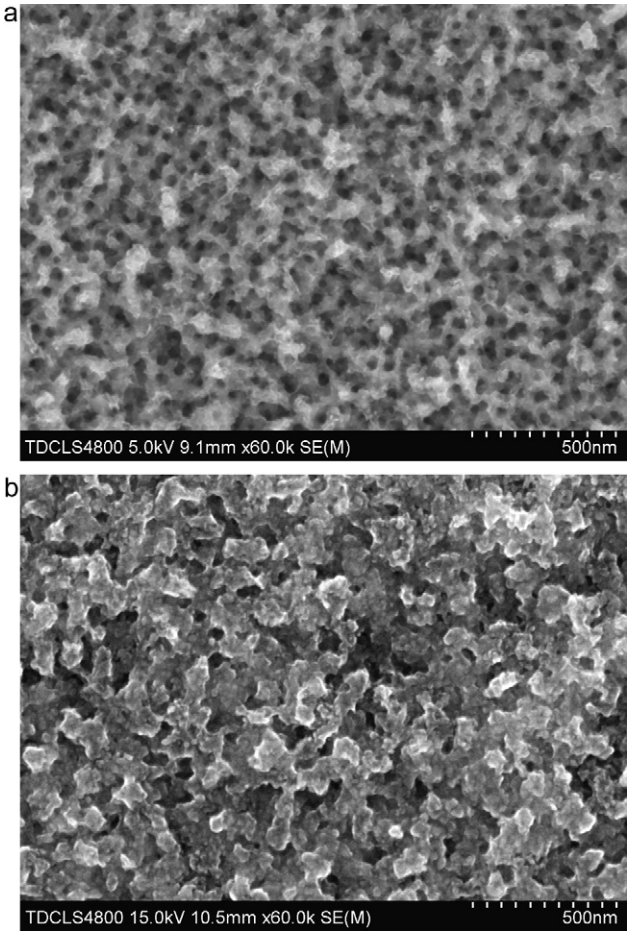

Fig. 1. SEM images of (a) OS and (b) HS.

Ti–Cu amorphous alloy are abbreviated as BS, OS and HS respectively.

Surface morphology was observed using Hitachi S-4800 scanning electron microscopy (SEM). Electrochemical measurements were carried out using an electrochemical station (Gamry Reference 600, USA). The conventional three-electrode system was used. BS, OS, or HS was utilized as working electrode. All potentials were given with respect to SCE. All electrochemical tests were conducted at constant temperature (T = 298 K).

Electrocatalytic activities of all samples towards ethylene glycol (EG) oxidation were studied in an acid medium containing 1.0 M EG + 1.0 M H_2SO_4, and an alkaline medium containing 1.0 M EG + 2.0 M NaOH, respectively. Cyclic voltammetry (CV) were performed ranging from −1 V to 1 V at a scanning rate of 50 mV/s. Chronoamperometry (CA) were carried out for 600 s. Electrochemical impedance spectroscopy (EIS) was measured with the amplitude of 10 mV in the frequency range from 10,000 Hz to 0.1 Hz.

3. Results and discussion

Fig. 1 shows SEM images of OS and HS. Nanopores of OS are uniformly distributed as shown in Fig. 1a. The mean diameter of nanopores is about 50 nm. The thickness of pore walls is about 70 nm. After heated at 573 K for 30 min, the amount of nanopores decreases as shown in Fig. 1b. The nanopores' size becomes non-uniform, ranging from 30 nm to 150 nm. The thickness of pore walls increases to about 100 nm. In short, heat treatment destroys the appropriate nanoporous structure of OS.

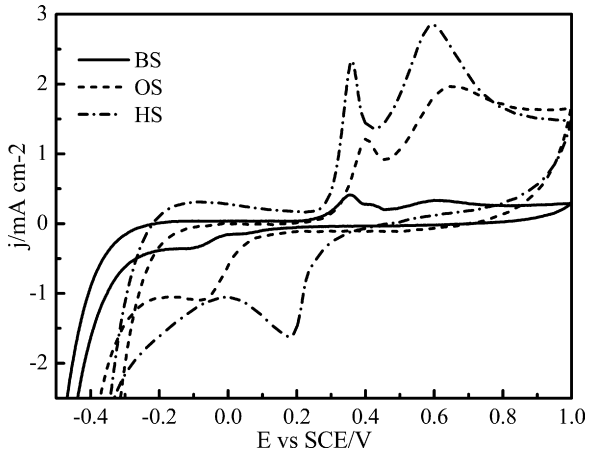

Fig. 2. CV plots of EG oxidation in 1.0 M EG + 1.0 M H_2SO_4.

Fig. 2 shows CV curves of three different samples in acid medium. Electrocatalytic activities of different samples can be evaluated through their peak current density in CV curves. In the forward CV scan, EG oxidation peak current density of three samples follows this order: HS > OS > BS. BS exhibits insignificant peaks. It implies that BS does not have electrocatalytic activity generally. Two main peaks are observed for OS and HS. The first current peak locates at 0.40 V for OS, whereas 0.36 V for HS. The second current peak locates at 0.65 V for OS, whereas 0.59 V for HS. Higher peak current density of HS at lower potentials indicates that EG oxidation activity of HS is higher than that of OS.

It is well established that the electrocatalytic oxidation of small organic molecules follow at nanostructured Pt/Pd electrodes [1,5,19,20,22,23,44]. In CV curves of methanol electro-oxidation on these catalysts in acid media, an anodic current peak appears in the forward scan and another anodic peak appears in the reverse scan [1,22]. The oxidation peak in forward scan is contributed to methanol dissociative adsorption and formation of strongly adsorbed intermediates [1]. The oxidation peak in negative scan is caused by reoxidation of these adsorbates via interaction with chemisorbed oxygen containing species (OH_{ads}) [44]. In case of ethanol and other alcohols electro-oxidation, C–C bond breaking interaction is an extra influent factor [23]. The same situation supposed to be considered for EG electro-oxidation. EG electro-oxidation in acid media is depicted as follows. At lower potentials, EG oxidizes incompletely to C_2 byproducts which dominate the reaction on blocked catalyst. In addition, CO_2 formation is limited by the formation of adsorbed oxy-species, which are required for oxidation of CO_{ads} produced by dissociative EG adsorption [6].

Below 0.25 V, the oxidation current is negligible in both CV curves of OS and HS. It is mainly because active sites are poisoned by adsorption of EG onto catalysts surface. As potentials increase, the oxidation current increases rapidly. It suggests that significant EG oxidation occurs. The first current density peaks at 0.40 V for OS and 0.36 V for HS are corresponding to the oxidation of freshly chemisorbed species from EG adsorption. Several electrons are transferred from each EG molecule. Some reaction intermediates such as glycolate, glyoxal, glycolic acid are generated [23,45]. These byproducts are strongly adsorbed onto the catalysts surface, and then poison nanoporous catalysts on further oxidation of EG. As electro-potential increases from 0.45 V, the oxidation current densities of OS and HS increase rapidly again, and reach a maximum at 0.65 V for OS and 0.59 V for HS, respectively. Further oxidation of as-formed intermediates and direct oxidation of residual EG occur on the catalysts surface. Final products such as carbonate and carbon dioxide are obtained [46,47]. More electrons are transferred from each EG molecule in the latter process than that in the former

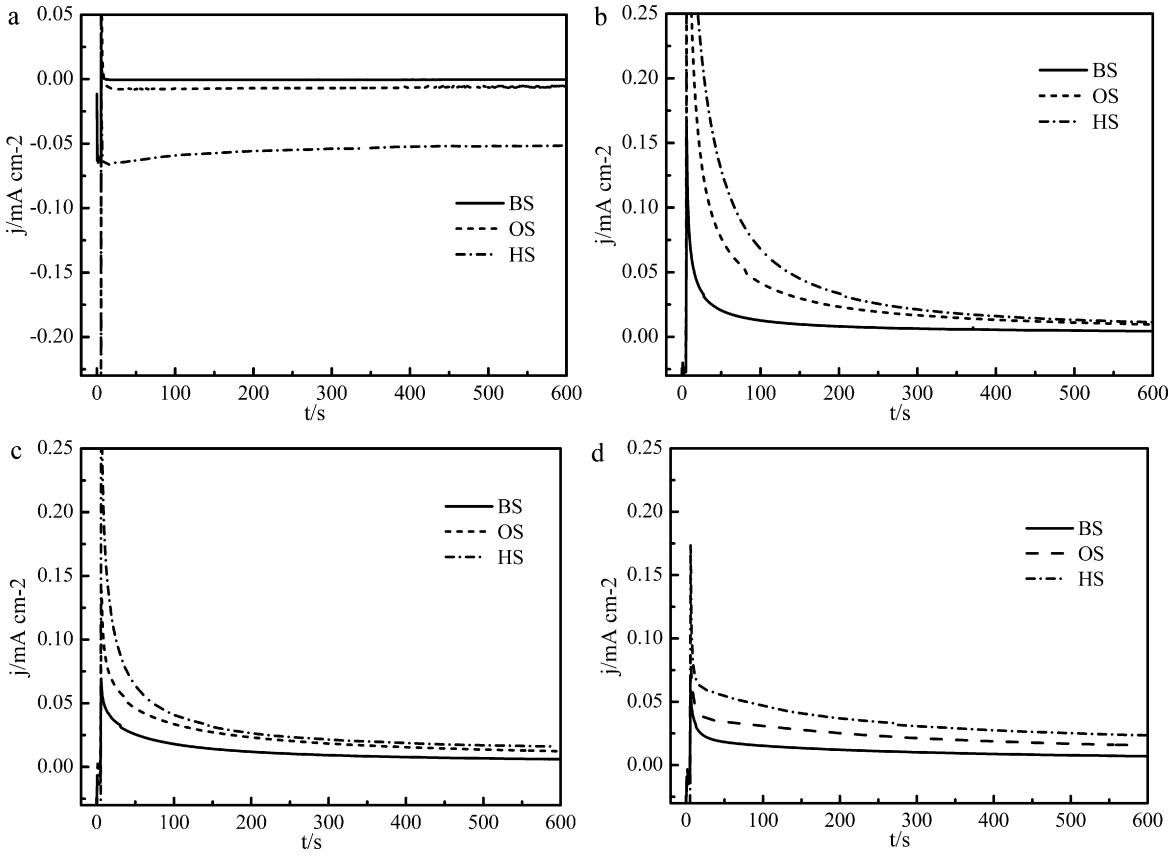

Fig. 3. CA plots of EG oxidation at (a) 0.3 V, (b) 0.5 V, (c) 0.7 V and (d) 0.9 V in 1.0 M EG + 1.0 M H_2SO_4.

one. Thus current densities of the second peak are higher than that of the first one.

Nanoporous structure provides large surface areas and a great deal of active sites in a catalytic reaction [28]. Thus EG and its reaction products can be adsorbed and distributed onto nanoporous catalysts conveniently. Finally nanoporous structure results in better catalytic performance of OS and HS than BS. In addition, EG oxidation activity of HS is higher than that of OS. It is probably caused by HS' better stability after heat treatment and partly bigger pore size comparing to OS. Poisoning species generated during EG oxidation can be desorbed from surface of HS effectively. Thus the electrocatalytic process on HS is more efficacious than that on OS.

To understand more about the better performance of OS and HS, CA measurements in acid medium are performed under potentials of 0.3, 0.5, 0.7, and 0.9 V, with a initial potential of 0.05 V. Current density–time responses at four different potentials are presented in Fig. 3. All the samples exhibit negative current densities at 0.3 V (Fig. 3a), which is quite the opposite of them at the other three potentials (Fig. 3b–d). Absolute values of current densities at all the potentials follow: HS > OS > BS. The negative current under 0.3 V is mainly caused by adsorption of EG molecules to samples surface. 0.3 V is too low to enable oxidation of EG. At the other three potentials, all the samples display a gradual current decay before stable current densities are attained. It is attributed to the adsorption of EG and poisoning intermediates onto the catalysts surface towards EG electro-oxidation reaction. Main tendency of three samples all over the experiment period is in well agreement with the above CV results.

Fig. 4 depicts CV curves of EG electro-oxidation of three samples in alkaline medium. Between −0.3 and 0.1 V, there are two peaks in the forward scan for OS and HS, which is not similar with that in previous studies [2,11,21,28]. The first current peak locates at −0.17 V for OS, while −0.14 V for HS. The second current peak locates at 0.04 V for OS, while 0.02 V for HS. The order of peak current density follows: HS > OS > BS. Below 0.1 V, BS does not seem to have EG catalytic activity, EG electro-oxidation efficiency of HS is higher than that of OS. As electro-potential increases to higher than 0.1 V, BS and OS display broad current densities peaks, while HS exhibits negative current density. It suggests that no EG oxidation happens on HS above 0.1 V basically. Heat treatment prohibits EG oxidation at potentials higher than 0.1 V.

In alkaline media, it is well known from previous studies that EG oxidation peaks on nanostructured Pt/Pd catalyst appear at more negative potentials than those in acid media [2]. A similar phenomenon is observed for methanol electrocatalytic

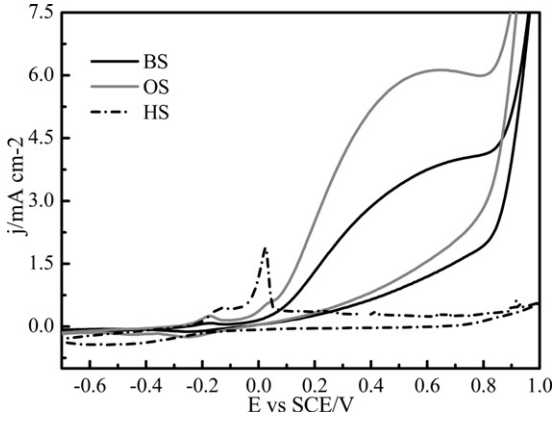

Fig. 4. CV plots of EG oxidation in 1.0 M EG + 2.0 M NaOH.

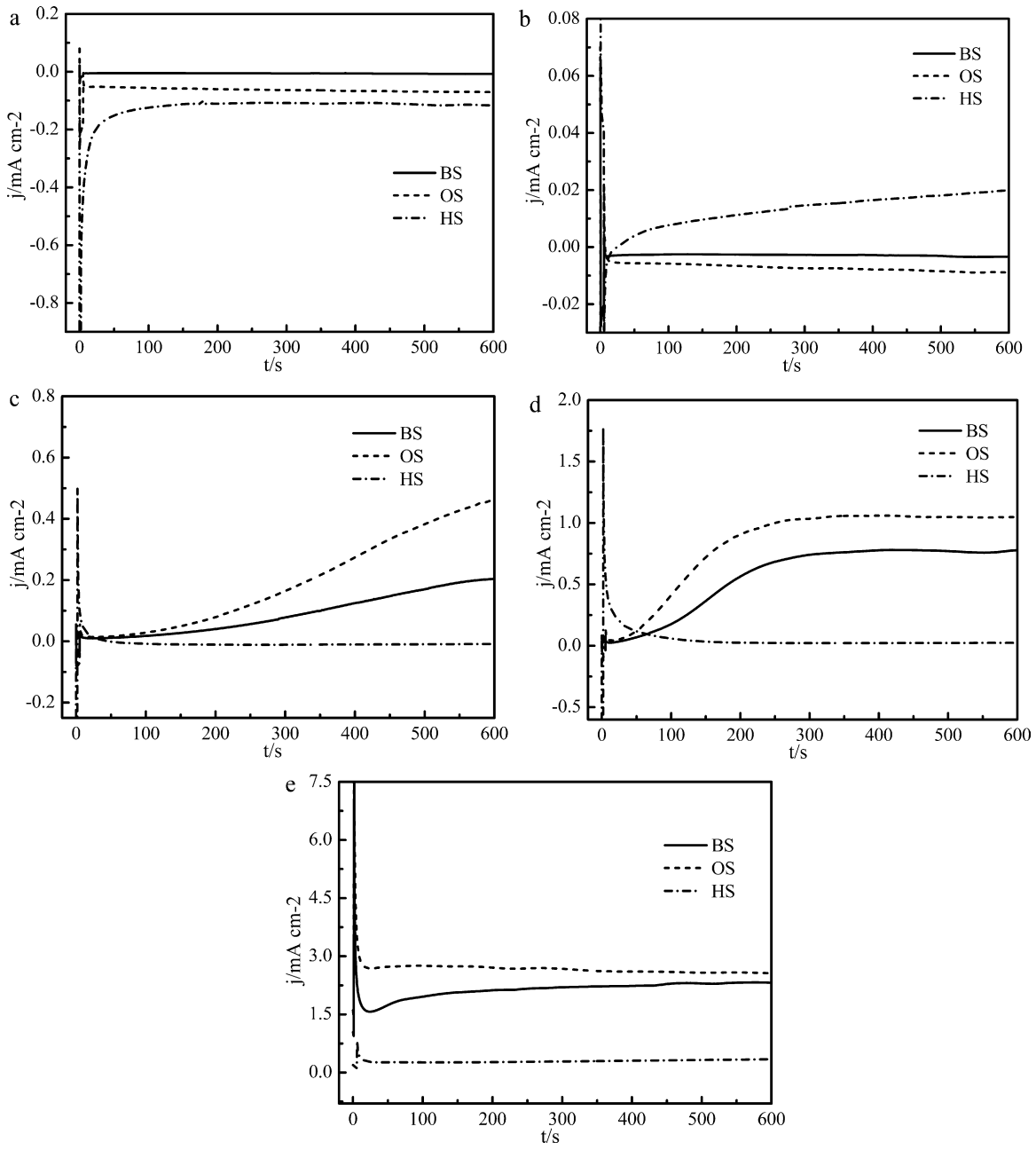

Fig. 5. CA plots of EG oxidation at (a) −0.3 V, (b) −0.1 V, (c) 0.1 V (d) 0.3 V and (e) 0.5 V in 1.0 M EG + 2.0 M NaOH.

oxidation. The peak located in forward scan is produced due to oxidation of freshly chemisorbed species [48,49]. The reverse oxidation peak is primarily correlated with removal of carbonaceous species which are not completely oxidized in the forward scan [11,21,49–51], or still related to oxidation of methanol molecules in the electrolyte [52,53]. Considered the deficiency of Pt catalysts, Hosseini investigated electrocatalytic behavior of Ni/TiO_2/Ti electrode towards methanol oxidation in alkaline media [12]. There appeared to be an oxidation peak at about 0.35 V and a reduction peak at about 0.24 V in CV scan.

Two main peaks appear at lower potentials in alkaline medium (Fig. 4) than in acid medium (Fig. 2). It suggests that EG oxidation reaction takes place more easily in alkaline medium than that in acid medium. Possible reason is that electrons can be transferred from EG molecule more conveniently in presence of OH^- [54,55]. Indeed, oxidation of EG in alkaline media consumes OH^- groups, results in formation of various oxidation products such as glycolate, oxalate or carbonate, Eqs. (1)–(3) [24].

$$(CH_2OH)_2 + 5OH^- \rightarrow CH_2(OH)COO^- + 4H_2O + 4e^- \quad (1)$$

$$(CH_2OH)_2 + 10OH^- \rightarrow (CO_2)_2^{2-} + 8H_2O + 8e^- \quad (2)$$

$$(CH_2OH)_2 + 16OH^- \rightarrow 2CO_3^{2-} + 10H_2O + 12e^- \quad (3)$$

The first peak is possibly corresponding to formation of preliminary oxidation products from EG, following Eq. (1). As potentials increase, these intermediates get further oxidation, and residual EG is oxidized to more ultimate products, following Eqs. (2) and (3). Thus current density of the second peak is higher than that of the first one. Electrocatalytic activity order of three samples below 0.1 V in alkaline medium is the same as that in acid medium, as investigated above.

Above 0.1 V, the displayed broad peaks of BS and OS are possibly corresponding to a complicate oxidation reaction of EG and EG

products residues. Various reactions are probably involved in this process, such as oxidation of glyoxal, oxalic acid and direct oxidation of EG to carbonate and/or carbon dioxide [56]. Insignificant electro-oxidation activity of HS is probably correlated to apparent blocking of nanopores by adsorbed OH^- and EG reaction products due to its small amount of nanopores comparing to OS.

In addition, oxidation current above 0.1 V in alkaline medium is much higher than that in acid medium. It implies that OS owns superior catalytic activity in alkaline medium. OH^- is adsorbed onto nanoporous structure to form a kind of precursor oxide which can effectively promote EG oxidation. Loading high potential will strengthen the oxidation process. The intermediate products will be oxidized to carbonate or other final products continuously with increasing potential. This thorough oxidation will avoid a possible catalyst poisoning and improve the efficiency of nanoporous structure as a kind of electrocatalyst.

Fig. 5 shows CA plots performed at −0.3, −0.1, 0.1, 0.3, and 0.5 V with an initial potential of −0.5 V in alkaline medium. At −0.3 V (Fig. 5a), it is the same as the phenomenon at 0.3 V in acid medium (Fig. 3a). −0.3 V is too negative to enable EG oxidation of all the samples. More negative current on OS and HS than it on BS is corresponding to stronger adsorption of EG onto nanoporous samples surface. At −0.1 V, an interesting finding is observed, current densities on BS and OS are negative, whereas positive on HS (Fig. 5b). The explanation supposed to be, EG oxidation current is bigger than EG adsorption current for HS, whereas smaller for BS and OS. As electro-potential increases to 0.1 V, the current density on HS is higher than that on BS and OS at the beginning 25 s. Then the current density on HS decreases to a stable value in a short time, but it increases continually on BS and OS all over the experiment period (Fig. 5c). This current density–time response indicates that 0.1 V is not stable for EG electro-oxidation on BS and OS. Oxidation and adsorption of EG are continuously, accompanied by desorption of EG electro-oxidation products on catalysts surface. At 0.3 V, current densities do not reach to a stable value until 250 s on BS and OS (Fig. 5d). It indicates that the desorption of EG oxidation products is less powerful than that at 0.1 V. Stable current density is attributed to a balance of oxidation and adsorption–desorption of EG and its reaction products. At 0.5 V, stable current densities on BS and OS (Fig. 5e) are obtained in a shorter time than that requires at 0.1 and 0.3 V. It implies that the desorption ability of EG oxidation products from catalyst surface becomes much poorer. Overall current density–time responses of three samples measured in alkaline medium are in well accordance with the CV results. BS does not show significant catalytic activity below 0.1 V, while HS does not display obvious catalytic performance above 0.1 V.

EIS technique is a powerful and non-destructive method to study and analyze the surface processes on an electrode. As discussed above, OS and HS exhibit apparent catalytic activity towards EG electro-oxidation in acid medium, OS shows high electrocatalytic activity in alkaline medium as well. EIS is used to investigate the kinetic of EG oxidation on nanoporous catalyst in depth.

Fig. 6 displays Nyquist complex-plane impedance spectra of EG electro-oxidation on OS and HS in acid medium at five different potentials (0.3, 0.4, 0.5, 0.6, and 0.7 V). A single capacitive arc is observed on OS at each potential as shown in Fig. 6a. In principle, a large arc diameter in Nyquist impedance spectra is corresponding to a small capacitance constant and a big Faraday current impedance [2,19]. Thus it is difficult to overcome the large energy barrier in an electrode reaction. And finally a large arc diameter results in a slow electrode reaction rate. At 0.3, 0.4, 0.5, and 0.6 V, the arc diameter maintains at a low value. It suggests oxidation of EG on OS takes place easily and effectively. As potential increases to 0.7 V, an increase of arc diameter indicates a smaller rate of OS surface reaction than that at the above potentials.

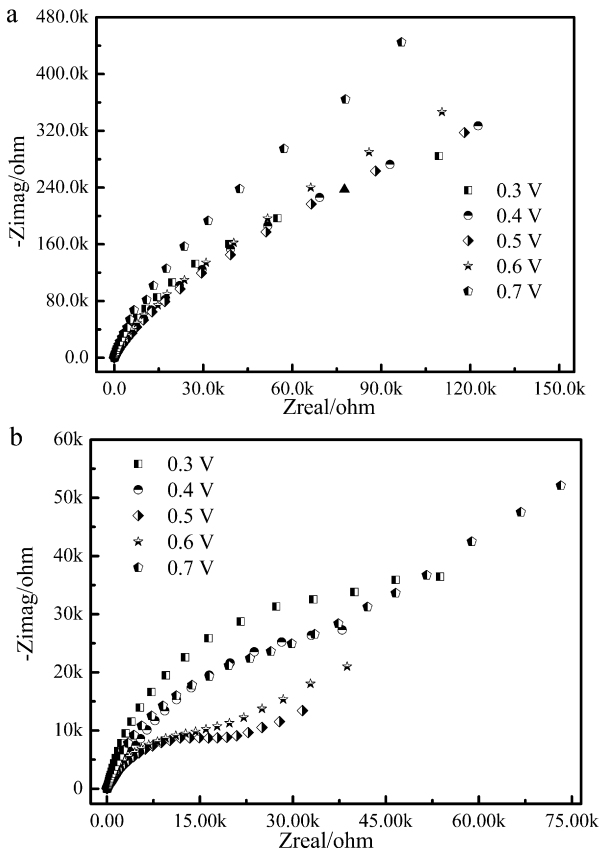

Fig. 6. EIS plots of (a) OS and (b) HS measured at different potentials in 1.0 M EG + 1.0 M H_2SO_4.

A different phenomenon is observed For HS as shown in Fig. 6b. A single capacitive arc appears in Nyquist graphs at 0.3 and 0.4 V. Increase in electrode potential leads to small arc diameter, illustrating reaction rate of EG oxidation increases. At 0.5, 0.6, and 0.7 V, a capacitive arc in high frequency region and a straight line in low frequency region are observed. Diameter of the capacitive arc in high frequencies at 0.5 and 0.6 V is further decreased than that at 0.4 V. It suggests that EG electro-oxidation is more effective at such potentials. The straight line in low frequencies is correlated with the diffusion of EG and its reaction products between electrode surface and electrolyte. When the potential increases up to 0.7 V, the arc diameter becomes larger. It implies that EG oxidation becomes slower again.

Compared the Nyquist plots of OS with HS, the arc diameter of HS at each potential is much smaller than that of OS. It indicates that the rate of EG oxidation on HS is higher than that on OS. At higher potentials, the smaller pore size of OS prohibits diffusion of EG and its reaction products. Thus there appears to be a less significant straight line in low frequencies of OS than that of HS. In total, these measured EIS results of OS and HS in acid medium are in well accordance with the above CV results.

Fig. 7 shows the Nyquist complex-plane impedance spectra of EG electro-oxidation on OS in alkaline medium at eight different potentials (−0.3, −0.2, −0.1, 0, 0.1, 0.2, 0.3 and 0.4 V). At −0.3 V, a single capacitive arc with a large diameter is observed. It implies insignificant reaction happens at this potential. As potential increases to −0.2 V, Nyquist plot appears to be a deformed capacitive arc, its arc diameter decreases in a vast scale. It suggests the ongoing of adsorption and electro-oxidation reaction of EG on OS. At −0.1 and 0 V, diameter of capacitive arc in high frequency region get further decreased with electrode potential increased. It indicates that EG oxidation accelerates. In lower frequencies, an

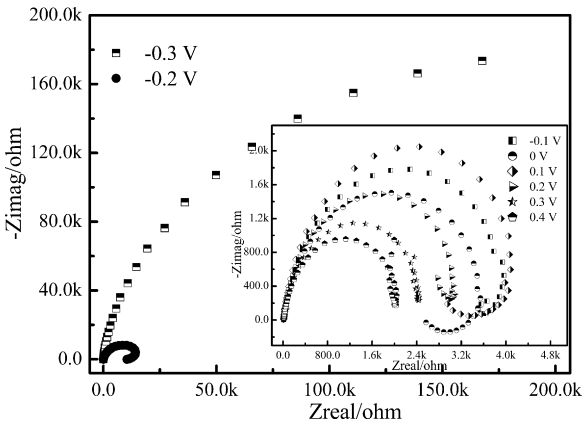

Fig. 7. EIS plots of OS measured at different potentials in 1.0 M EG + 2.0 M NaOH.

inductive arc is observed at each potential, which is caused by adsorption effect. Larger diameter of the inductive arc at 0 V indicates larger adsorption resistance than that at −0.1 V. At 0.1 V, the diameter of the capacitive and inductive arc becomes larger. It is possibly attributed to strongly adsorbed initial EG reaction products which cannot be oxidized and desorbed on catalyst surface at this potential. Starting from 0.2 V, the capacitive arc diameter in high frequencies continues to decrease. It suggests that the oxidation of adsorbed EG and their primarily oxidation products speeds up continuously. The second capacitive arc at low frequencies, which is caused by adsorption effect as well, supposed to be further oxidation of the first stage oxidation products. Decrease in diameter of the second arc indicates that rate of the second stage oxidation becomes lower. EIS analytical results of OS towards EG electro-oxidation in alkaline medium are in well agreement with the above CV results on all accounts.

4. Conclusion

Nanoporous Ti–Cu amorphous alloy exhibits excellent electrocatalytic activities towards EG electro-oxidation both in acid and alkaline mediums. In acid medium, original nanoporous Ti–Cu amorphous alloy performs two main oxidation peaks at 0.40 and 0.65 V in forward CV scan. According to CV, CA and EIS results, heat treatment improves catalytic activity of nanoporous Ti–Cu amorphous alloy in acid medium. In alkaline medium, EG oxidation on original nanoporous Ti–Cu amorphous alloy occurs more easily for apparently more negative oxidation peak potentials (−0.17 and 0.04 V). Heat treated nanoporous Ti–Cu amorphous alloy exhibits higher catalytic activity than the original one below 0.1 V, and depressed catalytic activity above 0.1 V. The second capacitive arc appears in Nyquist complex-plane impedance spectra of OS proves its better electrocatalytic activity. Probable electro-oxidation mechanism of EG on nanoporous Ti–Cu amorphous alloy is demonstrated as a sequent process of oxidation and adsorption–desorption of EG and its reaction products.

Acknowledgements

This work was supported by Key Projects in the Tianjin Science & Technology Pillar Program (09ZCKFGX29100) and National Natural Science Foundation of China (50901051). The infra-structural supports from the Tianjin University are also acknowledged.

References

[1] Z.H. Wang, G.Q. Gao, H.F. Zhu, Z.D. Sun, H.P. Liu, X.L. Zhao, Int. J. Hydrogen Energy 34 (2009) 9334.
[2] Y.Y. Feng, W.P. Yin, Z. Li, C.D. Huang, Y.X. Wang, Electrochim. Acta 55 (2010) 6991.
[3] V. Livshits, M. Philosoph, E. Peled, J. Power Sources 178 (2008) 687.
[4] E. Peled, V. Livshita, T. Duvdevani, J. Power Sources 106 (2002) 245.
[5] C. Jeyabharathi, P. Venkateshkumar, J. Mathiyarasu, K.L.N. Phani, Electrochim. Acta 54 (2008) 448.
[6] M. Chojak Halseid, Z. Jusys, R.J. Behm, J. Electroanal. Chem. 644 (2010) 103.
[7] J.C.M. Silva, R.F.B. De Souza, L.S. Parreira, E. Teixeira Neto, M.L. Calegaro, M.C. Santos, Appl. Catal. B 99 (2010) 265.
[8] C. Kulp, X.X. Chen, A. Puschhof, S. Schwamborn, C. Somsen, W. Schuhmann, M. Bron, ChemPhysChem 11 (2010) 2854.
[9] W.Z. Li, C.H. Liang, W.J. Zhou, J.S. Qiu, Z.H. Zhou, G.Q. Sun, Q. Xin, J. Phys. Chem. B 107 (2003) 6292.
[10] J.H. Ma, Y.Y. Feng, J. Yu, D. Zhao, A.J. Wang, B.Q. Xu, J. Catal. 275 (2010) 34.
[11] Y. Wang, X. Wang, C.M. Li, Appl. Catal. B 99 (2010) 229.
[12] M.G. Hosseini, M.M. Momeni, M. Faraji, Electroanalysis 22 (2010) 2620.
[13] Y.T. Kim, K. Ohshima, K. Higashimine, T. Uruga, M. Takata, H. Suematsu, M. Tadaoki, Angew. Chem. Int. Ed. 45 (2006) 407.
[14] Y.C. Zhao, X.L. Yang, J.N. Tian, F.Y. Wang, L. Zhan, Int. J. Hydrogen Energy 35 (2010) 3249.
[15] Y.Q. Liang, Z.D. Cui, S.L. Zhu, Y. Liu, X.J. Yang, J. Catal. 278 (2011) 276.
[16] Q. Wang, B.Y. Geng, B. Tao, J. Power Sources 196 (2011) 191.
[17] C. Coutanceau, S. Brimaud, C. Lamy, J.M. Leger, L. Dubau, S. Rousseau, F. Vigier, Electrochim. Acta 53 (2008) 6865.
[18] S. Raghu, R.G. Nirmal, J. Mathiyarasu, S. Berchmans, K.L.N. Phani, V. Yegnaraman, Catal. Lett. 119 (2007) 40.
[19] R.G. Freitas, E.C. Pereira, Electrochim. Acta 55 (2010) 7622.
[20] H.Z. Yang, J. Zhang, K. Sun, S.Z. Zou, J.Y. Fang, Angew. Chem. Int. Ed. 49 (2010) 6848.
[21] A.S. Polo, M.C. Santos, R.F.B. de Souza, W.A. Alves, J. Power Sources 196 (2011) 872.
[22] S.L. Wei, D.C. Wu, X.L. Shang, R. Fu, Energy Fuels 23 (2009) 908.
[23] R.B. de Lima, V. Paganin, T. Iwasita, W. Vielstich, Electrochim. Acta 49 (2003) 85.
[24] V. Bambagioni, M. Bevilacqua, C. Bianchini, J. Filippi, A. Marchionni, F. Vizza, L.Q. Wang, P.K. Shen, Fuel Cells 10 (2010) 582.
[25] Y.J. Hu, J. Jin, P. Wu, H. Zhang, C.X. Cai, Electrochim. Acta 56 (2010) 491.
[26] J. Sebera, H. Hoffmannova, P. Krtil, Z. Samec, S. Zalis, Catal. Today 158 (2010) 29.
[27] K. Mohsen, A.K. Mohammad, Carbon 48 (2010) 3131.
[28] X.G. Wang, W.M. Wang, Z. Qi, C.C. Zhao, H. Ji, Z.H. Zhang, J. Power Sources 195 (2010) 6740.
[29] L.Y. Chen, T. Fujita, Y. Ding, M.W. Chen, Adv. Funct. Mater. 20 (2010) 2279.
[30] C.X. Xu, L. Wang, X.L. Mu, Y. Ding, Langmuir 26 (2010) 7437.
[31] J. Erlebacher, M.J. Aziz, A. Karma, N. Dimitrov, K. Sieradzki, Nature 410 (2001) 450.
[32] Y. Ding, Y.J. Kim, J. Erlebacher, Adv. Mater. 16 (2008) 1897.
[33] J. Snyder, K. Livi, J. Erlebacher, J. Electrochem. Soc. 155 (2008) C464.
[34] D.V. Pugh, A. Dursun, S.G. Corcoran, J. Mater. Res. 18 (2003) 216.
[35] D.V. Pugh, A. Dursun, S.G. Corcoran, J. Electrochem. Soc. 152 (2005) B455.
[36] X.G. Wang, Z. Qi, C.C. Zhao, W.M. Wang, Z.H. Zhang, J. Phys. Chem. C 113 (2009) 13139.
[37] Q. Zhang, Z.H. Zhang, Phys. Chem. Chem. Phys. 12 (2010) 1453.
[38] C.C. Zhao, Z. Qi, X.G. Wang, Z.H. Zhang, Corros. Sci. 51 (2009) 2120.
[39] J.C. Thorp, K. Sieradzki, L. Tang, P.A. Crozier, A. Misra, M. Nastasi, D. Mitlin, S.T. Picraux, Appl. Phys. Lett. 88 (2006) 033110.
[40] J.S. Yu, Y. Ding, C.X. Xu, A. Inoue, T. Sakurai, M.W. Chen, Chem. Mater. 20 (2008) 4548.
[41] W.H. Wang, C. Dong, C.H. Shek, Mater. Sci. Eng. R 44 (2004) 45.
[42] H.S. Chen, C.E. Miller, Rev. Sci. Instrum. 41 (1970) 1237.
[43] S.L. Zhu, J.L. He, X.J. Yang, Z.D. Cui, L.L. Pi, Electrochem. Commun. 13 (2011) 250.
[44] O.V. Cherstiouk, A.N. Gavrilov, L.M. Plyasova, I.Y. Molina, G.A. Tsirlina, E.R. Savinova, J. Solid State Electrochem. 12 (2008) 497.
[45] P.A. Christensen, A. Hamnett, J. Electroanal. Chem. 260 (1989) 1101.
[46] E.M. Belgsir, E. Bouhier, H.E. Yei, K.B. Kokoh, B. Beden, H. Huser, J.-M. Leger, Electrochim. Acta 36 (1991) 1157.
[47] O.V. Cherstiouk, E.R. Savinova, L.A. Kozhanova, V.N. Parmon, React. Kinet. Catal. Lett. 69 (2000) 331.
[48] Z.P. Sun, X.G. Zhang, Y.Y. Liang, H.L. Li, J. Power Sources 191 (2009) 366.
[49] Y.W. Lee, S.B. Han, K.W. Park, Electrochem. Commun. 11 (2009) 1968.
[50] R.N. Singh, A. Singh, Anindita, Int. J. Hydrogen Energy 34 (2009) 2052.
[51] Z.L. Liu, X.H. Zhang, L. Hong, Electrochem. Commun. 11 (2009) 925.
[52] Q.G. He, W. Chen, S. Mukerjee, S.W. Chen, F. Laufek, J. Power Sources 187 (2009) 298.
[53] M. Sevilla, C. Sanchis, T. Valdes-Solís, E. Morallon, A.B. Fuertes, Electrochim. Acta 54 (2009) 2234.
[54] N. Dalbay, F. Kardigan, J. Electroanal. Chem. 296 (1990) 559.
[55] V. Bambagioni, C. Bianchini, J. Filippi, W. Oberhauser, A. Marchionni, F. Vizza, R. Psaro, L. Sordelli, M.L. Foresti, M. Innocenti, ChemSusChem 2 (2009) 99.
[56] M. Ureta-Zanartu, C. Yanez, M. Paez, G. Reyes, J. Electroanal. Chem. 405 (1996) 159.